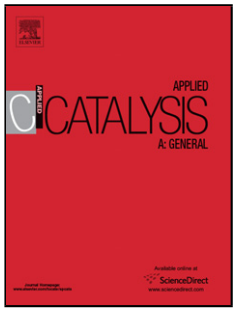

Title: Bio-nanohybrid catalysts based on L-leucine immobilized in hydrotalcite and their activity in aldol reaction

Author: Dana-Georgiana Crivoi Ronald-Alexander Miranda Elisabetta Finocchio Jordi Llorca Gianguido Ramis Jesús E. Sueiras Anna M. Segarra Francisco Medinaa

PII: S0926-860X(16)30140-5
DOI: http://dx.doi.org/doi:10.1016/j.apcata.2016.03.018
Reference: APCATA 15810

To appear in: *Applied Catalysis A: General*

Received date: 29-1-2016
Revised date: 11-3-2016
Accepted date: 17-3-2016

Please cite this article as: Dana-Georgiana Crivoi, Ronald-Alexander Miranda, Elisabetta Finocchio, Jordi Llorca, Gianguido Ramis, Jesús E.Sueiras, Anna M.Segarra, Francisco Medinaa, Bio-nanohybrid catalysts based on L-leucine immobilized in hydrotalcite and their activity in aldol reaction, Applied Catalysis A, General http://dx.doi.org/10.1016/j.apcata.2016.03.018

Bio-nanohybrid catalysts based on L-leucine immobilized in hydrotalcite and their activity in aldol reaction

Dana-Georgiana Crivoi,[a,b] Ronald-Alexander Miranda,[a,b*] Elisabetta Finocchio,[c] Jordi Llorca,[d,e] Gianguido Ramis,[c] Jesús E. Sueiras,[a,b] Anna M. Segarra,[a,b] and Francisco Medina[a,b*]

[a]Departament d'Enginyeria Química, Universitat Rovira i Virgili, Av. Països Catalans, 26, Campus Sescelades, Tarragona 43007, Spain

[b]EMaS-Centro de Investigación en Ingeniería de Materiales y Micro/nanoSistemas, Campus Sescelades, Tarragona 4300, Spain

[c]Dipartamento di Ingegneria Civile, Chimica e Ambientale , Università di Genova, P.le J.F.Kennedy 1, Genoa 16129, Italy

[d]Institut de Tècniques Energètique, Universitat Politècnica de Catalunya, Diagonal 647, ed. ETSEIB, Barcelona 08028, Spain

[e]Center for Research in NanoEngineering (CRnE-UPC). Universitat Politècnica de Catalunya, Pasqual i Vila 1-15, Barcelona 08028, Spain.

[*]E-mail: ronaldalexandermiranda@hotmail.com , francesc.medina@urv.cat

Graphical abstract

Bio-nanohybrid catalysts based on L-leucine immobilized in hydrotalcite and their activity in aldol reaction

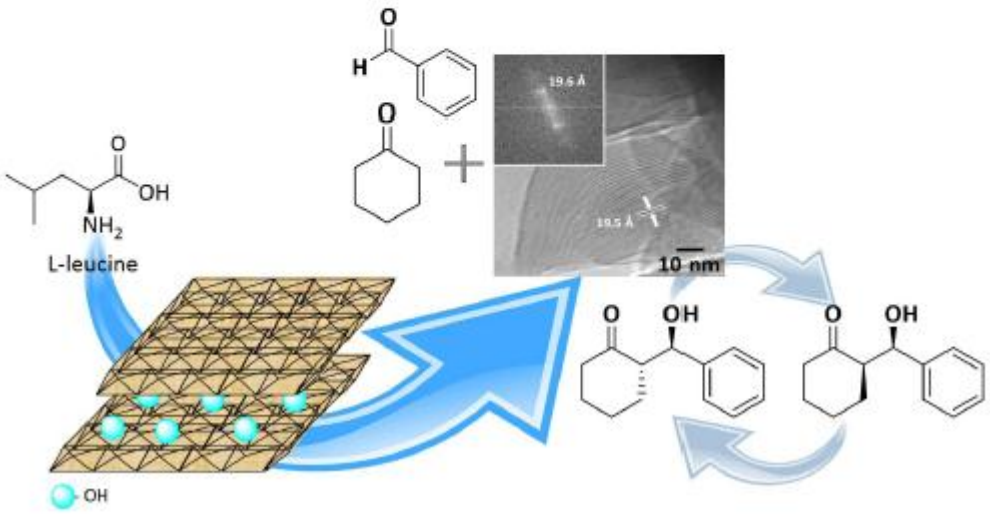

Highlights:

- The organic/inorganic interactions between L-leucine immobilized into hydrotalcites were studied
- By reconstruction method, the anionic form of L-leucine is immobilized in the interlayer space while by anionic exchange, both zwitterionic and anionic forms are immobilized
- These nanohybrid materials are more active in the asymmetric aldol reaction than the mere L-leucine
- Modulating reaction conditions (solvent, type of nanohybrid used, time) can lead to different reaction outcome

Nanohybrid materials based on L-Leucine (L-Leu) and hydrotalcites (HT) were prepared by the ion-exchange and reconstruction method, under mild synthesis conditions. The location, amount and the form of the immobilized L-Leu are affected not only by the time of synthesis, but also by temperature and ultrasound treatment. The XRD results demonstrate that the immobilization occurs in either a vertical or oblique orientation with respect to the HT layers. The catalytic activity of these materials was tested in the aldol addition reaction of cyclohexanone with different aromatic aldehydes, affording mainly the *syn*-diastereomer. Furthermore, the present study demonstrates that both diastereo- and enantioselectivity can be easily modulated by the appropriate combination of nanohybrid catalyst, solvent and reaction time.

Keywords: Asymmetric catalysis, Hydrotalcite, Immobilization, L-Leucine, Nanohybrid materials

1. Introduction

Nowadays, considerable attention is focused on the synthesis of nanohybrid materials, which exhibit new and better properties than the corresponding constituent materials. Research into and understanding the organic/inorganic interaction between bioactive molecules and the surface of inorganic materials have led to their use in many biochemical applications[1] or as catalysts [2] and drug delivery carriers [3], although these interactions remain only partially understood. Many bioactive molecules (e.g. peptides, amino acids, proteins, etc.) are anions under neutral and basic pH, so they can easily be immobilized in positively charged solids. Examples of such solids are the hydrotalcites (HTs), a family of naturally occurring layered clays with low or null toxicity, good biocompatibility and a high anion swelling capacity. These properties make HTs interesting materials for applications in the pharmaceutical field [4], cosmetics [5], catalysis [6] or even medical field [7].

The anionic exchange properties of HTs transform these materials in excellent candidates for the immobilization of amino acids (AAs). Starting with 1997 when Whilton *et al*. studied the immobilization of aspartic and glutamic acid in the interlayer space of layered double hydroxides through coprecipitation method [8], a series AAs have been immobilized into HT materials by means of three general methods: coprecipitation [9-12], anionic exchange [12-15] and reconstruction method [16, 17]. Regarding the nature of the interaction, it is now clear that the immobilization of AAs in HTs structures is pH-dependent, although other factors should be taken into account: the kind of HT, the synthesis and the physical and chemical properties of the AAs.

AAs are organocatalysts which display several advantages such as non-toxicity, easy manipulation and stability and have been widely used in the asymmetric aldol reaction [18]. For example, Córdova *et al*. obtained *anti* diastereoselectivity in a direct asymmetric aldol reaction between cyclohexanone and *p*-NO_2-benzaldehyde using a series of AAs [19]. Wu *et al.* used a threonine derivative in the aldol addition reaction, producing the *anti*-diastereomer when cyclohexanone was the substrate and *syn*-isomer in the case of hydroxyacetone [20]. Similar results were obtained by Barbas [21], Lu [22] and Gong [23]. Itoh *et al*. observed that in the presence of L-*t*-Leu compounds with *syn* diastereoselectivity were obtained in the case of cyclopentanone, cycloheptanone and cyclooctanone and with *anti* diastereoselectivity when cyclohexanone was used [24]. Thus, obtaining the *syn*-product when cyclohexanone is used as substrate seems to be a challenge. Moreover, AAs used in their natural form can react with aromatic aldehydes to form the corresponding immonium salts which, by decarboxylation, will form a stable side-product [24, 25].

In this study, we present the synthesis of nanohybrid materials based on L-Leu immobilized in HTs. We studied different synthetic procedures and their effects on the nature of the inorganic/organic interaction in order to

evaluate: i) the role of the immobilization time on one hand, and the relationship between the immobilization speed and the strength and kind of basic centres in the HT on the other hand; ii) the role of the HT precursor in the immobilization process and iii) the nature of the AA structure in the immobilization process. To achieve this goal, the nanohybrid materials were synthesized using the anion-exchange and reconstruction method and the organic/inorganic interactions were investigated by EA, ICP, XRD, FT-IR, Raman, ^{13}C, ^{27}Al MAS NMR and thermal evolution using TG/DTA analyses.

The new nanohybrid materials were tested in the aldol addition reaction of cyclohexanone with different aromatic aldehydes. The synergistic effect between the bio-organic guest (L-Leu) and the inorganic host (HTs) proved to play an important role in modulating both the diastereoselectivity and enantioselectivity of the final product. Herein, we report that the *anti-syn* selectivity depends not only on the nature of the catalyst but also on the solvent used.

2. Experimental

2.1 General

All chemicals and solvents were commercially available (Aldrich Chemical, Fluka) and used without further purification/drying unless otherwise mentioned.

Molecular formulae were calculated from the results of elemental analyses (EA) and inductively coupled plasma analyses (ICP). EA were performed using an elemental analyser EA-1108 C.E. instrument from Thermo Fisher Scientific with a Mattler Toledo MX5 microbalance. The analyses were carried out using atropine as a standard and Vanadium as an additive to facilitate combustion. ICP analyses were performed in an ICP-OES Spectro Arcos FHS16 Instrument.

The N_2-physisorption analysis of BET surface areas and average pore diameters were performed in a QuadStar Quantachrome surface analyser at 77 K. Before analysis all the samples were degassed in vacuum at 393 K for 12 h.

Powder X-ray diffraction (XRD) patterns of the samples were performed on a Bruker-AXS D8-Discover diffractometer with a 2θ angle ranging from 3º to 70º. The samples were dispersed onto a low background Si (510) sampler holder. The data were collected with an angular step of 0.03º at 5s per step and sample rotation. CuKα radiation (λ = 1.54056 Å) was obtained from a copper X-ray tube operated at 40 kV and 40 mA. The crystalline phases were identified using JCPDS files. The interlayered spaces were analysed with the reflection bands of the (003) and (006) and calculated using the Bragg law.

Fourier transform infrared spectra (FT-IR) were recorded with Nicolet Nexus Fourier Transform instrument equipped with a DTGS KBr detector. Each analysis was performed using 100 scans in the range 4000–400 cm^{-1}. Pure powders diluted in KBr pressed disks (about 1% w/w) were used for the analysis of skeletal vibrations. OMNIC software provided by ThermoElectron Corporation was used for spectra analysis.

Raman spectra were obtained using a Renishaw Raman via reflex instrument. The polarized radiation (λ=785 nm) of a Ranishaw diode laser of 500 mW was used. A Laica DM2500 optical microscope was used to determine the part of the sample analysed. The RamaScope was calibrated using a silicon wafer. The focus (maximum opening 100%) and power (50%) were carefully optimized in order not to alter the sample during measurement. The spectral resolution was 2 cm^{-1} with an exposure time of 10 s and 5 accumulations for each run.

^{13}C and ^{27}Al Magic Angle Spinning-Nuclear Magnetic Resonance (MAS-NMR) spectra were obtained on a Varian Mercury VXR-400S spectrometer operating at 104.2 MHz with a pulse width of 1 ms. A total of 4,000 scans were collected with a sweep width of 100 kHz and an acquisition time of 0.2 s. An acquisition delay of 1s between successive accumulations was selected to avoid saturation effects. ^{13}C MAS NMR spectra were recollected using tetramethylsilane (TMS) as reference.

High-resolution transmission electron microscopy (HRTEM) was performed with a JEOL 2010F instrument equipped with a field emission source, working at an acceleration voltage of 200 kV. The point-to-point resolution of the microscope was 0.19 nm, and the resolution between lines was 0.14 nm.

Thermogravimetric Analyses and Differential Thermal Analyses (TGA/DTA) were measured on a TGA7 instrument from Perkin Elmer. The analyses were carried out using a sample amount of 10 mg in an N_2 atmosphere. The heating rate was 10 ºC.min^{-1} within the range 30-900 ºC.

The products were characterized by ^{1}H-NMR using a Varian NMR System 400 MHz and HPLC-DAD (Diode Array Detector G1315D) Agilent Technologies and HPLC-RID 10A (Refractive Index Detector) Shimadzu using CHIRALPACK IA column (250*4.6 mm ID).

2.2 Synthesis of hydrotalcite materials (HTs)

Mg-Al HTs (Mg/Al molar ratio 2) containing nitrates and chloride anions were synthesized by the coprecipitation method at room temperature and pH=10. The materials obtained were named HT_{NO3} and HT_{Cl} respectively. After the drying process, HT_{Cl} was sonicated for 1 hour, while HT_{NO3} was decomposed by calcination at 450 ºC overnight in air. The calcined HT (HT_{cc}) was rehydrated in an inert atmosphere

using decarbonated water and ultrasound treatment for 1 hour. The materials obtained were named HT_{Clus} and HT_{rus} respectively.

2.3 Synthesis of LL/HT materials

2.3.1 Anionic-exchange method (method A)

Two procedures were used to synthesize LL/HT_x-Ay materials, where x is the type of HT used (HT_{rus} or HT_{Clus}) and y indicates the procedure followed. In the first case, 500 mg of HT was added to a solution containing 320 or 160 mg (2.4 or 1.2 mmol, respectively) of L-Leu. The mixture was stirred for 30 minutes at room temperature (method A1). In the second case, 500 mg of HT was added to a solution containing 840.4 mg (6.4 mmol) of L-Leu. The mixture was stirred for 3 hours at 80 ºC (method A2). An Ar atmosphere and deionized-decarbonated water were used in all cases. Materials synthesized by the anionic exchange method were named LL/HT_{rus}-A1, LL/HT_{Clus}-A1, LL/HT_{rus}-A2 and LL/HT_{Clus}-A2.

2.3.2 Reconstruction method (method R)

Two procedures were used to synthesize LL/HT_x-Ry materials (where x is the type of HT and y indicates the procedure followed), in both cases using 250 mg of HT_{cc} added to a solution containing 736.9 mg (5.6 mmol) of L-Leu. In the first procedure, L-Leu-HT_{cc} mixture was first treated by sonication for 1 hour and then the slurry was stirred for another 3 hours at 80 ºC. The material obtained was named LL/HT_{rus}-R1 (method R1). Alternatively, HT_{cc}-L-Leu mixture was stirred for 3 hours at 80 ºC (method R2). The material obtained was named LL/HT_r-R2. Table 1 summarizes the synthetic methods used in the present article.

2.4 Typical procedure for the aldol reaction of cyclohexanone

H_2O (25 mmol) and cyclohexanone (1.5 mmol) were added to a mixture containing aldehyde (0.5 mmol), catalyst (2.5 mol % L-Leucine with respect to ketone) in DMSO (2ml) or Toluene (2 ml) and the resulting mixture was stirred at room temperature. After a defined period of time, brine was added and the reaction mixture was extracted several times with CH_2Cl_2. Due to its high boiling point, DMSO cannot be removed by vacuum distillation. In this context, DMSO was diluted by adding brine solution (NaCl solution) to: (i) facilitate the separation of aqueous and organic phases after adding CH_2Cl_2 and (ii) destroy any emulsion that might be formed during the extraction process The organic layer was dried with $MgSO_4$ and concentrated under vacuum. The reaction mixture was purified by column chromatography using silica

gel and hexane/ethyl acetate 3/1 as eluent. The conversion was determined by either isolation or ^{1}H-NMR analysis and the enantiomeric excess by HPLC analysis.

3. Results and discussion

3.1 Catalyst characterization

3.1.1 Textural properties of HT and LL/HT materials

Nanohybrid materials based on L-Leu and HTs were synthesized by two methods (anion-exchange and reconstruction) to understand the nature of immobilized L-Leu in the HT structure: the location and ionic state of this AA. Table 2 shows the L-Leu/Al^{3+} molar ratio, BET surface area and interlayer space of the different HTs and nanohybrid materials synthesized.

Cavani *et al.* explained that the introduction of large anionic species in the interlayer space of a hydrotalcite material, either by anionic exchange method or reconstruction method, will be reflected in an increase in the interlayer space of the HT [26]. In accordance with Cavani's findings, we have observed an increase in the HT's gallery height in all the materials where the L-Leu was immobilized inside the hydrotalcite (entries 7, 9 and 10, Table 2). When the anionic exchange method was used at room temperature for 30 minutes (LL/HT_{rus}-A1 material) no increase in the gallery height of the support was observed, even though a ratio of 0.44 L-Leu/Al^{3+} was obtained (entry 5, Table 2). This demonstrates that the AA was preferably immobilized on the edges of the HT_{rus} layers. An increase in the amount of immobilized AA will produce a loss of crystallinity, observed in the XRD patterns presented in the Supporting Information (Figure I).

Increasing the time and temperature of synthesis to obtain LL/HT_{rus}-A2 increased the amount of immobilized L-Leu to 1.09 mol L-Leu/mol Al^{3+}, producing an interlayer space to 19.5 Å (entry 7, Table 2). This finding shows that both time and temperature have an effect on the swelling of the HT structure, allowing the immobilization of L-Leu molecules in its interlayer space. The loss of crystallinity in all nanohybrid materials was due to the decrease of the layers' lengths by the ultrasound effect.

The same conclusions can be drawn from the HRTEM images of the precursor and the nanohybrid materials. In the case of HT_{rus}, the image shows aggregated layers up to about 100 nm in length, with an interlayer space around 7.6 Å as deduced by FT analysis (Figure 1a). The LL/HT_{rus}-A1 material (Figure 1 b) has a similar morphology as the HT_{rus}, demonstrating once again that using method A1 the L-Leu is not found inside the HT layers, but on the edges. The distinctive morphology observed in the case of LL/HT_{rus}-

A2 (Figure 1 c) compared to that of HT_{rus} proves the intercalation of the LL inside the layers and not on the edges of the material.

To sustain our previous findings, we have conducted several control experiments using hydrotalcites containing Cl^-; these HTs have a lower basicity than the HT_{rus} [27] and do not favour the immobilization of hydrophobic amino acids through anionic-exchange method [17]. Indeed, in both cases (LL/HT_{Clus}-A1 and LL/HT_{Clus}-A2) no increase in the interlayer space was observed, demonstrating that the AA did not exchange the chloride ions (entries 6 and 8, Table 2). Moreover, the very low amount of L-Leu computed by EA and ICP analysis suggest that the HT_{Clus} surface is not basic enough to immobilize a larger amount of amino acid.

Materials synthesized by reconstruction method (LL/HT_{rus}-R1 and LL/HT_r-R2) exhibited a significant shift in the d_{003} peak position compared with the HT_{rus} XRD pattern (Figure I in Supporting Information). Furthermore, the interlayer space of these nanohybrid materials increased to around 20 Å (entries 9 and 10, table 2). The HRTEM images (Figure 2) do not conserve the layer morphology of their HT precursor and revealed interlayer spacing at 22.5-22.6 Å, indicating that the immobilization of L-Leu molecules occurs in the interlayer space of the HT. In addition to the basal planes at 22.5-22.6 Å, both LL/HT_{rus}-R1 and LL/HT_r-R2 materials present lattice fringes at 14.8-14.9 Å.

Nakayama *et al.*[17] immobilized L-leucine into HT using a reconstruction method and observed an increase in the gallery height of 9.8 Å corresponding to the thickness of two L-leucine molecules arranged in a bilayer structure. The material LL/HT_{rus}-A1 presented a similar gallery height as the normal HT which demonstrate that the immobilized L-leucine is found at the edges of the HT in a horizontal position with respect the HT layer. On the other hand, the material LL/HT_{rus}-A2 has a gallery height of 14.3 Å. The approximate length of a L-leucine molecule is of 7.109 Å, thus the interlayer distance observed for LL/HT_{rus}-A2 can be explained by a bilayer structure of L-leucine oriented in a vertical position with respect to the HT layer.

The high gallery heights observed in the case of nanohybrids synthesized using reconstruction method suggest that the bilayer structure of L-leucine contain the amino acids in both vertical and oblique orientation with respect to the HT layer.

BET surface area results (found in Table 1) are in agreement with the previous discussion: when L-Leu is immobilized inside the HT-structure the surface area decreases considerably compared to the parent material. The LL/HT_{rus}-R1 and LL/HT_r-R2 materials presented a more significant decrease in surface area

loss than the ones by A1 and A2 method. This suggests that the AA is found within the aggregates formed by the disordering of the layers (during ultrasound treatment) and their position hinders the adsorption of N_2, reducing the available surface area of the materials (see the N_2 adsorption-desorption isotherms –Figure II and III in Supporting Information).

3.1.2 FT-IR and Raman spectroscopy

Skeletal FT-IR and Raman spectra of L-Leu, HT_{Clus} and HT_{rus} can be found in Supporting Information (Figure IV) along with the detailed explanations of the specific bands of each parent material. Moreover, the thermal decomposition curves of the nanohybrid precursors can be found in Supporting Information (Figures VII and VIII).

3.1.2.1 Nanohybrids synthesized by the anionic exchange method

To better understand and evaluate the interaction of L-Leu with the HT surface, we used the control materials based on HT_{Clus}. The FT-IR (up) and Raman (bottom) spectra of LL/HT_{Clus}-A1 and LL/HT_{Clus}-A2 do not present strong evidence of immobilized L-Leu (Figure 3a and 3b, respectively). In the case of the LL/HT_{Clus}-A1, it is difficult to draw conclusions because of the very low content of L-Leu present in the sample (entry 6, Table 2). The FT-IR spectrum of LL/HT_{Clus}-A2 material showed some differences compared to its HT precursor. At high frequency, two bands at 2957 and 1581 cm^{-1} can be observed due to the small amount of L-Leu molecules interacting with HT material. At low frequency, the differences in the bands at 970, 790 and 553 cm^{-1} compared to the spectrum of the HT precursor suggest changes in the Al-OH species. These changes could result from the presence of a higher amount of OH^- anions and to some L-Leu molecules immobilized in the HT structure. However, the Raman spectrum of LL/HT_{Clus}-A2 does not present any evidence of immobilized L-Leu (Figure 3b, bottom).

The FT-IR spectra of nanohybrid materials (Figure 4 up) synthesized using HT_{rus} material showed, besides the vibration bands due to the HT precursor, some sharp components attributable to the L-Leu, demonstrating that the AA was successfully immobilized. LL/HT_{rus}-A1 and LL/HT_{rus}-A2 spectra exhibit the bands corresponding to the C-H stretching mode at 2975 (ν_{CH}) and 2870 cm^{-1} (ν_{CH3}), slightly shifted with respect to the bands of pure Leu, confirming the immobilization of the L-Leu. The FT-IR spectrum of LL/HT_{rus}-A1 material exhibits the $\nu_{a(COO-)}$ and $\nu_{s(COO-)}$ stretching at 1560 and 1407 cm^{-1} respectively, while bands attributable to the NH_3^+ group were not clearly detected (Figure 4a, up). These findings, together with the XRD and HRTEM prove that the immobilization process was mainly caused by an anionic exchange between anionic L-Leu and the OH^- groups located on the HT edges. Similarly, in the FT-IR spectrum of

LL/HT_{rus}-A2 material, the $\nu_{a(COO-)}$ stretching at 1560 cm^{-1} indicates the presence of the anionic L-Leu (Figure 4b up). An exhaustive study of this spectrum also shows small bands at 1581, 1610 and 1516 cm^{-1} due to COO^- and NH_3^+ groups of the zwitterionic L-Leu. The decrease in intensity of the broad band specific to water OH stretching mode and of the band ascribed to CO_3^{2-} species at 1384 cm^{-1} in both LL/HT_{rus}-A1 and LL/HT_{rus}-A2 materials suggests that the incorporation of the L-Leu in the materials causes the displacement of physisorbed water and the competition with the adsorption of CO_3^{2-} anions [28, 29].

The Raman spectra of LL/HT_{rus}-A1 and LL/HT_{rus}-A2 materials present bands at 2886, 1227 and 835 cm^{-1} due to CH stretching modes (Figure 4a and 4b bottom, respectively). The form in which L-Leu is found in the LL/HT_{rus}-A1 is difficult to be identified due to the low intensities of the RAMAN bands (Figure 4a, bottom). In the LL/HT_{rus}-A2 Raman spectrum, the bands at 1471 and 1455 cm^{-1} attributable to the COO^- group in pure L-Leu shifted to 1464 and 1449 cm^{-1} respectively (Figure 4b, bottom). In addition, the relative intensity of both bands changes after immobilization, suggesting the presence of two kinds of COO^- groups in L-Leu: anionic and zwitterionic. Changes in their relative intensity also indicate that both COO^- are interacting with the HT structure, anions located in the interlayer space and/or other L-Leu molecules. Moreover, the relative intensity of the band at 1061 cm^{-1} due to CO_3^{2-} species decreased after L-Leu immobilization, confirming the reduced incorporation of atmospheric CO_2 in the HT structure.

In general, the FT-IR and Raman spectra of nanohybrid materials synthesized by anion exchange method show that the immobilization process cannot occur on the surface of the HT material. In addition, the high basicity of the HT_{rus} can favour the immobilization of L-Leu in its anionic form until the accessible OH^- groups in the HT edges are compensated. This interaction protects the material from CO_3^{2-} incorporation. Nevertheless, the decrease in the strong basic centres in the material causes the formation of zwitterionic AA (L-Leu detected through diagnostic bands ascribed to NH_3^+) which could interact with Al-OH species, structural water, OH^- groups still available in the material or other zwitterionic L-Leu molecules.

3.1.2.2 Nanohybrids synthesized by the reconstruction method

The FT-IR (up) and Raman (bottom) spectra of nanohybrid materials synthesized by the reconstruction method are presented in Figure 5. The FT-IR spectrum of LL/HT_r-R2 (Figure 5b up) presents broad bands at 3064 cm^{-1} and around 2700 cm^{-1} assigned to vibration modes of the NH_3^+ group. In addition, the band at 2130 cm^{-1} is also due to a combination of asymmetric deformation and hindered rotation of NH_3^+ groups [30]. The relative intensity of all the bands assigned to the NH_3^+ group decreased following immobilization,

in comparison to the spectrum of the pure Leu, probably due to H-bonds between the NH_3^+ group and the oxygen atoms of the HT layers. Bands due to νa(COO^-) and νs(COO^-) stretching were also detected as in pure L-Leu. Although the intercalation of some anionic L-Leu cannot be completely ruled out, immobilized L-Leu using HT_{cc} without ultrasound treatment clearly occurs mostly in its zwitterionic form.

The Raman spectrum of LL/HT_r-R2 material presents bands at 2886, 1227 and 835 cm^{-1} attributable to CH and CC stretching modes (see Figure 5b, bottom). The band at 1455 cm^{-1} due to the COO^- group in pure L-Leu spectrum remains unchanged after the immobilization process, while the band at 1471 cm^{-1} shifted to 1464 cm^{-1} after immobilization. Moreover, the detection of weak and broad band at 1186 cm^{-1} and shifted band at 1125 cm^{-1} due to NH_3^+ group demonstrated the immobilization of both zwitterionic and anionic L-Leu molecules.

FT-IR and Raman spectra of LL/HT_{rus}-R1 presented no significant differences compared to LL/HT_{rus}-A2 (see Figure 5a and Figure 4b, respectively). The band due to νa(COO^-) stretching shifted to lower frequencies from 1581 to 1560 cm^{-1}, while the bands corresponding to NH_3^+ stretching vibrations were not detected. This suggests that the immobilization of the L-Leu occurs in its anionic form, in agreement with Aisawa *et al.* findings [9]. Only two differences in the Raman spectrum of LL/HT_{rus}-R1 were detected in comparison with the LL/HT_{rus}-A2 spectrum: the band at 1297 cm^{-1} due to the deformation mode of the -OH in plane and the band at 1187 cm^{-1} due to the NH_3^+ group were not detected. This indicated that the immobilization mainly occurred in an anionic form.

In conclusion, the FT-IR and Raman spectra of the nanohybrid materials synthesized using the reconstruction method show that using ultrasound treatment during the synthesis the L-Leu molecules are immobilized in their anionic form.

All the information extracted from the Raman and FT-IR analysis of the nanohybrid materials is summarized in Table 3.

3.1.3 MAS NMR Spectroscopy

To investigate the nature of the interaction between L-Leu and the HTs using MAS NMR spectroscopy, we have chosen the nanohybrid materials that contained the highest L-Leu/Al^{3+} molar ratio: LL/HT_{rus}-A2, LL/HT_{rus}-R1 and LL/HT_r-R2.

The typical ^{27}Al MAS-NMR spectrum of HT_{rus} presents an important signal at 9 ppm due to the octahedral coordinated Al and two small signals at 105 and 81 ppm attributable to extra framework tetrahedral Al atoms still present after rehydration process (see figure V in Supporting Information) [31-33].

Because none of the nanohybrid materials ^{27}Al MAS-NMR spectra had the signal at 9 pm sifted, demonstrates that the interaction of the immobilized L-Leu with the HT does not involve the Al atoms (entries 2, 3 and 4, Table 4).

The ^{13}C MAS-NMR spectrum of the pure L-Leu exhibits the typical signals of the zwitterionic form, mainly: a signal at 176 ppm due to the carboxylate group, signals at 55 and 44 pm corresponding to C_α and C_β respectively and a broad band at 26 ppm assigned to the C_γ and C_δ (entry 1, Table 4). The shifting of the carboxylate group signal from 176 ppm to 186 ppm in the case of LL/HT_{rus}-A2 and LL/HT_{rus}-R1 spectra (entries 2 and 3, Table 4) confirm that L-Leu was immobilized in the anionic form [16]. The ^{13}C MAS-NMR spectrum of the LL/HT_{rus}-A2 material presented also a less intense signal at 176 ppm, suggesting that some of the L-Leu is found in a zwitterion form (Supporting Information figure VI).

The same two signals were also observed in the case of LL/HT_r-R2 material (entry 4, Table 4), but the intensities were inversed, demonstrating that the L-Leu was immobilized mainly under the zwitterionic form.

3.2 Nature of the organic/inorganic interaction

The extensive and detailed characterization presented in the above section revealed that variations in the immobilization methods lead to materials with different characteristics, as it is summarized in Scheme 1.

Briefly, when the starting material was HT_{cc}, the L-Leu immobilization took place in the same time as the rearrangement of the HT. Ultrasound treatment (in the case of LL/HT_{rus}-R1 material) breaks the HT layers creating more basic sites, which, in the presence of water and L-Leu facilitate the immobilization process. The L-Leu is found in the anionic form between the HT layers. When the hybrid was synthesised without ultrasounds (LL/HT_r-R2 material), the L-Leu was immobilized in the interlayer space in both anionic and zwitterionic form, producing a catalyst with a higher crystallinity. Our results indicate that immobilization of the anionic L-Leu occurs by compensating the OH^- groups found in the HT interlayer space. The immobilization of zwitterionic L-Leu occurs by H-bonding between the $-NH_3^+$ group of the L-Leu with water and/or OH^- groups in the HT layers.

When the synthesis started with HT_{rus}, the temperature used was the crucial parameter. Thus, the synthesis carried out at 80 °C (material LL/HT_{rus}-A2) favoured the immobilization of L-Leu in the interlayer space by ionic exchange until all accessible centres were compensated, then the immobilization occurred by interactions between the zwitterionic L-Leu with water or OH^- anions located in the interlayer

space. When the HT_{rus} was simply stirred in the presence of L-Leu (LL/HT_{rus}-A1), immobilization occurred by anionic exchange of the OH^- anions located on the edge of the HT with the anionic L-Leu.

3.3 Asymmetric aldol reaction of cyclohexanone

T. Itoh *et al.*[24] reported the low activity of L-Leu in the aldol reaction of p-nitrobenzaldehyde with cyclohexanone in the presence of DMSO and water for seven days. Under these conditions, the reaction gave the corresponding β-ketoalcohol with a very low yield, moderate *anti* diastereoselectivity and high enantioselectivity towards the (2S,1'R)-aldol compound (entry 1, Table 5). The low activity is attributable to the cyclization of the imine intermediate (formed in the reaction between the amino acid and the aldehyde) followed by a decarboxylation, resulting in a stable 1,3-oxazolidine compound [25].

Rehydrated hydrotalcites have proven to possess high activity in several reactions, due to the presence of a large number of –OH groups which act as Brönsted basic sites and are presumed to be responsible for the catalytic activity of these materials. On this basis, the HT_{rus} was tested in the aldol reaction of different benzaldehyde-like compounds with cyclohexanone using the conditions mentioned by T. Itoh *et al.* [24] (Table 5). The HT_{rus} afforded high yields and efficiently controlled *syn*-selectivity when substituted aromatic aldehydes were used (entries 2, 5 and 8, Table 5), while the *anti*-selectivity was preferred in the case of benzaldehyde (entry 11, Table 5).

Using the same conditions, we tested L-Leu/HT_{rus} materials in the aldol reaction of the four chosen aromatic aldehydes. We used LL/HT_{rus}-R1 and LL/HT_{rus}-A2 as model catalyst due to the nature of AA immobilized (as mentioned in the previous section, in the R1 the L-Leu is present in the anionic form while in A2 in both zwitterion and anionic form). The manner in which the catalyst was prepared turned out to be crucially important in the reaction efficiency. Both catalysts yield good conversions in the reaction of 4-nitrobenzaldehyde (entries 3 and 4, Table 5) compared to the case when free L-Leu was used (entry 1, Table 5). Even though *sin* diastereoselectivity was preferred, the form in which L-Leu was immobilized greatly influenced the enantioselectivity. Thus, when L-Leu was present in the anionic form - LL/HT_{rus}-R1 – 90% ee for the *syn* isomer was obtain and only 60% ee for the *anti*. When L-Leu was present in both anionic and zwitterion form, the ee % of the *syn* diastereoisomer decreased to 71% while the ee% for *anti*-increased to 74%. In the case of 2-nitrobenzaldehyde the reaction done in the presence of LL/HT_{rus}-R1 afforded also the *syn*-diastereoisomer, but enantioselectivity was higher towards the *anti*-isomer (entry 6, Table 5). This shows that the steric hindrance of the nitric group found in ortho position and the anionic form of L-Leu play an important part in determining the enantioselectivity. A similar trend was observed when LL/HT_{rus}-A2 was used, exhibiting a lower stereoselectivity for the *syn* isomer. The second para-substituted aldehyde used in this study showed similar trends in both cases, but with a slighter increase in ee% for the *syn* isomer (entries

9 and 10, Table 5). A totally different behaviour was observed in the case of benzaldehyde: LL/HT_{rus}-R1 favoured the formation of the *syn* diastereoisomer, with good to moderate enantioselectivity for both diastereoisomers, while the LL/HT_{rus}-A2 favoured the *anti*-isomer but with practical no enantioselectivity and reverse ee % for the *syn* (entries 12 and 13, Table 5). All these results clearly show that both LL/HT_{rus}-R1 and LL/HT_{rus}-A2 are far better catalysts than pure L-Leu, employing the same conditions as T. Itoh *et al.* [24].

As control experiments, we have studied the catalytic activity of the physical mixture between L-Leu and the corresponding HT (calcined or rehydrated) for the aldol reaction between benzaldehyde and cyclohexanone (entries 14 and 15, Table 5). High conversions were obtained in both cases and the diastereoselectivity is similar to the one obtained with LL/HT_{rus}-A2. This catalytic behaviour indicates that part of the HT_{cc} is rehydrated in the reaction medium favouring the intercalation of the L-Leu to give the LL/HT_{rus}-A2 material. The XRD diffractograms of the physical mixture of HT_{cc} and L-Leu before and after the reaction, along with the XRD pattern of the LL/HT_{rus}-A2 can be found in Supporting Information. Interestingly, the trends of the ee% for *syn* and *anti* are similar to that of the corresponding catalysts, slightly higher in the case of HT_{rus} + LL and lower for the other physical mixture.

To evaluate the reusability and stability of the catalysts, we chose as substrate benzaldehyde, due to its unique behaviour in terms of diastereoselectivity and enantioselectivity. When LL/HT_{rus}-A2 was used and under the conditions proposed by T. Itoh *et al.* [24] the catalyst lost its activity after first run (entry 1, Table 6). In the LL/HT_{rus}-A2 material, L-Leu is found in both zwitterion and anionic form and due to the exothermic reaction that takes place during work-up (adding brine over reaction mixture) the amino acid is removed from the HT, decreasing thus the activity of the catalyst (figure XI in Supporting Information). Moreover, the Cl^- anions found in the brine solution are able to replace the vacant zones of the HT interlamellar space, leading to the formation of an inactive catalyst. The amino acid which is now free in solution will react with benzaldehyde leading to the formation of the corresponding 1,3-oxazolidine (figure XII in Supporting Information). The catalyst LL/HT_{rus}-R1 presented slightly higher activity in the second run compared to the other case, suggesting a stronger interaction between the anionic form of the amino acid and the HT interlamellar space than in the case of LL/HT_{rus}-A2 (entry 2, Table 6).

To avoid the use of NaCl, we repeated the reactions using toluene as solvent (entry 3 and 4, Table 6). In this case, two different behaviours were observed depending on the nature of the catalyst: when LL/HT_{rus}-A2 was used, an increase towards the *anti*-diastereoisomer can be observed over the three runs while, in the other case (LL/HT_{rus}-R1), an increase of the *syn*-diastereoisomer is observed. In terms of enantioselectivity, a slightly increase in ee% is detected for both isomers over the three runs, in the case of LL/HT_{rus}-A2, while when LL/HT_{rus}-R1 is used, a change

in enantioselectivity is observed for the *syn* diastereomer. These preliminary results suggest that the solvent plays an important part in the reaction pathway and might have an effect on the reaction enantioselectivity.

For an in-depth study of this process and to understand the reaction profile, we performed a 4h kinetic study of the aldol reaction between cyclohexanone and benzaldehyde under all the conditions mentioned above (catalysed by HT_{rus}, mechanical mixture between L-Leu and HT, LL/HT_{rus}-A2 and LL/HT_{rus}-R1 and the conditions mentioned by T. Itoh *et al.* [24]).

The first study was done using HT_{rus} as catalyst. (Figure 6). It is intriguing to note that, although the reaction was complete after only 1h, there is a continuous interchanging between the *syn* and the *anti* diastereoisomers. Miller *et al.* discovered a stereoisomeric system in which spontaneous enantiomeric enrichment occurred in a homogeneous mixture. They observed an amide isomerization proportional to the fluctuation of each diastereomer's enantiomeric ratio as the *cis-trans* equilibration occurred [34].

To explain the observed behaviour, we have to take into account the strong basic sites present in the HT_{rus} which can promote the reaction by subtracting an H atom in the α-position of the ketone compound [35]. Scheme 2 presents a possible mechanism of the *syn-anti* isomerization, where the cyclohexanone (1) will be in equilibrium with the enol form (2) in aqueous solvent and will react further with the benzaldehyde to give the corresponding aldol product (4). Due to the presence of the interlayer –OH groups and the water medium, H-bonds play an important role in stereoselectivity, favouring the *syn-an*ti inversion [36].

A different behaviour is observed when the reaction is carried out using the corresponding HT mixed with L-Leu. In the first case (Figure 7-A), two different catalysts are present in the reaction mixture: HT_{cc} and L-Leu. As HT_{cc} has lower basic sites than HT_{rus}, the aldol reaction will require longer time for completion. Additionally, the quantity of water present in the medium is able to rehydrate the HT material and thus, proceeding in the formation of LL/HT_{rus}-A2. The free amino acid is involved in three competitive processes: catalysing the formation of 1,3-oxazolidine compound, catalysing the aldol reaction and being involved in the immobilization process. At this point is difficult to know which form of L-Leucine is active in this experiment. Surprising, along the 4 h a slow decrease in the enantioselectivity of the reverse *anti* isomer is observed.

Furthermore, the system HT_{rus} + L-Leu is much more active giving a higher selectivity towards the aldol products (figure 7-B). In this case, three processes may occur simultaneously: formation of the 1,3 – oxazolidine, aldol reaction and immobilization of the AA. From all of them, the reaction system favours the immobilization of L-Leu on the HT_{rus} and thus, only a small portion of the L-leucine will be involved in the formation of 1,3-oxazolidine

compound and of the *anti* –aldol product (Figure 7-B – values in brackets). After 2 hours of reaction, the catalyst LL/HT_{rus}-A2 is already formed.

The degree of interchanging between *syn* and *anti*-isomers depends on the nature of the catalyst: in the case of LL/HT_{rus}-A2 during the first hour the *syn* diastereoisomer is present in a higher concentration than the *anti*, but in time its concentration decrease as it can be seen in Figure 8-A; on the other hand, when LL/HT_{rus}-R1 was used, the *anti* diastereoisomer is in excess from the beginning, and after 3h the conversion towards the *syn* diastereoisomer increases, as observed in Figure 8-B. Regarding the enantioselectivity, during the first 3 hours of reaction in the presence of LL/HT_{rus}-R1 the ee% remains constant for the *anti*-isomer (Figure 8-B – values in brackets) while there is no enantioselectivity for the *syn* diastereoisomer. In the case of LL//HT_{rus}-A2 a change in stereoselectivity is observed for the *syn* diastereomer and a slightly increase in enantioselectivity for the *anti* (Figure 8-A – values in brackets).

Figure 9 illustrates that the reaction proceeds slower in toluene than in aqueous DMSO and total conversion is achieved after 3h. The catalyst obtained through the anionic exchange method (Figure 9-A) behaves totally different when toluene is used and in the first 4h of reaction there is no interchanging between the diastereoisomers. In the same time, the enantioselectivity towards the other *syn* isomer remains constant, while the enantioselectivity of the *anti*-product is much lower than in the case were DMSO was used as solvent. In addition, when LL/HT_{rus}-R1 is used, after 2 h of reaction an inversion between the diastereoisomers is observed, while the ee% is increasing for the *syn* isomer and slightly decreases for the *anti* (Figure 9-B). As mentioned in the "Nature of the organic/inorganic interaction" section, when the catalyst is prepared through the A2 method, the active basic sites (interlamellar –OHs) are interacting with the L-Leu found in both anionic and zwitterion form. In a nonpolar solvent and with no water present, the LL/HT_{rus}-A2 catalyst is incapable of catalysing the interchanging between the diastereoisomers. Moreover, when only the anionic form of L-Leu is immobilized, as in the case of LL/HT_{rus}-R1, there are more –OH available, thus promoting the interchanging as can be seen in figure 9 B.

Literature presents several reactions done "in water" or "in the presence of water", the last being reported to increase the reactivity and stereoselectivity [37, 38]. In this context, we have performed the 4h kinetic study of aldol reaction in toluene and "in the presence of water", results being shown in Figure 10. Adding only a small amount of water in toluene completely changed the course of reaction. In both cases there was a high selectivity towards the *anti*-diastereoisomer, a very good enantioselectivity of this isomer and no enantioselectivity for the *sin* isomer (Figure 10 A and B). Our results show that the solute-solvent interactions are able to affect the stereochemical outcome of the aldol reaction even when a non-polar solvent is used.

Cordová *et al.* have shown that there are three possible mechanisms by which a free AA can catalyse the aldol reaction: the carboxylic acid catalysed enamine mechanism, the amino catalysed enamine mechanism and the enaminium catalysed mechanism, where the amino acid is found in the zwitterion form [39]. These mechanisms cannot be applied when the amino acid is immobilized between the layers of hydrotalcites, due to the presence of the secondary material which is also active in aldol reaction. So far, our results show that when the reaction carried out in polar solvent (DMSO) the conversion and enantioselectivity are low, but when non-polar solvents are used with a very small quantity of water, the catalytic activity is improved. This might be explained as follows: in the non-polar medium, the substrate has to penetrate into the layers of the HT and, as Vijaikumar *et al.*[2] shown, the polar nature of the interlayer will help the catalysis as well as the chiral induction of the AA to occur. Scheme 3 presents a possible mechanism of the aldol reaction catalysed by the LL/HT catalysts. Firstly, the amino group of L-Leu activates the ketone by a nucleophilic attack at the carbonyl carbon, generating an enaminium intermediate. The *syn* diastereoselectivity is influenced by the highly basic character of the hydrotalcite. The –OH groups of the HT interact with the aldehyde, polarizing it and facilitating the nucleophilic attack of the enamine, which, in presence of water will give the corresponding *syn*-adduct. Amedjkouh showed that bases can be used as co-catalysts in the adol reaction to enforce *syn*-selectivity retaining a high level of enantioselectivity, and unbounded amino acids usually favour the formation of *anti*-aldol product [40]. Next, the *syn* isomer can undergo isomerization, as presented in Scheme 2.

The HT interlayer space provides the perfect environment for the L-leucine, increasing its activity by promoting enantioselectivity through an oriental attack. The activity of this bifunctional catalyst is enhanced by the polar medium found in HT galleries and by the presence of water. As Gong *et al.* showed, the double hydrogen bonding activation of carbonyl functionality influence the transition state, exhibiting high stereoselectivity towards the *syn*-aldol product if the reaction is not quenched in the first 4h [41].

The behaviour of these new bio-hybrid catalysts is extremely complicated and certainly require further investigation for a complete comprehension on how the solvent, time of reaction and the way the catalyst is prepared affect the activity and enantioselectivity.

4. Conclusions

The controllable basicity, the "memory effect" and the ion exchange property make HTs excellent materials to immobilize amino acids and study their organic/inorganic interactions. In this context, we have obtained four new materials based on L-leucine and Mg-Al HT by means of two procedures: reconstruction method and anionic exchange method.

In the anionic exchange method, the immobilization involves mainly the anionic form of L-Leu and an increase in the synthesis time and temperature permits the swelling of the HT material, allowing the immobilization to occur inside the HT layers. An excess of L-Leu in the reaction media will favour the immobilization on the edges of the HT structure. The use of ultrasound treatment during reconstruction method not only increased the basic sites of the HT, but also favoured the immobilization of L-Leu inside its layers. The absence of this treatment will favour the AA intercalation by means of H-bonding between its structure and the inorganic anions found in the interlayer space.

Regardless of the intercalation method used, we have shown that the immobilization cannot occur through the interaction between the Al^{3+} atoms from the HTs structure and the anionic L-Leu. Moreover, according to the XRD results, the immobilization could occur in a vertical or oblique orientation with respect to the HT layers (Scheme 1). When the AA was immobilized in the zwitterionic form, the orientation depended on the chemical environment in the interlayer space from the HT.

These new materials were more active in the asymmetric aldol reaction of cyclohexanone with different aromatic aldehydes (up to 99% conversion and moderate to good enantioselectivity) than the corresponding physical mixture and the mere amino acid. When the reaction was carried out in aqueous DMSO, the catalysts lost their activity after the first run, due to the exothermic reaction that takes place during work-up (adding brine over reaction mixture) when L-Leu is removed from the HT. Just by using toluene, both conversion and selectivity were highly improved.

The kinetic studies we performed have shown that the aldol reaction between cyclohexanone and benzaldehyde carried out using these new catalysts, toluene and "in the presence of water" is completed in less than 4 h, achieving 99% yield and maintaining the enantioselectivity in the case of the *anti*-diastereomer.

The mechanism of reaction is very complex and involves simultaneous activity of the two parts of the catalyst: the hydrotalcite and the immobilized L-Leu. If in general the free amino acid favours the formation of the *anti*-isomer, the presence of the basic HT leads to the formation of the *syn*-isomer. Moreover, depending on the conditions of reaction, the *syn* and *anti*-diastereoisomer can undergo isomerization.

Therefore, the different synthesis protocols and different reaction conditions can be employed to obtain a specific aldol-product. Further studies will be carried out to exploit the potential advantages and properties of these LL/HT_{rus} catalysts in the asymmetric aldol reaction of cycloketones. This future work will focus on

understanding how the solvent, time and the way the catalyst is prepared affect the activity and enantioselectivity, making use of theoretical computations and possible transition states.

Acknowledgements

Dana-Georgiana Crivoi is grateful to the Spanish Government's MECD for the FPU predoctoral grant.

Notes and references

[1] J.-H. Choy, S.-J. Choi, J.-M. Oh, T. Park, Clay minerals and layered double hydroxides for novel biological applications, Appl. Clay. Sci., 36 (2007) 122–132.
[2] S. Vijaikumar, A. Dhakshinamoorthy, K. Pitchumani, L-Proline anchored hydrotalcite clays: An efficient catalyst for asymmetric Michael addition, Appl. Catal., A, 340 (2008) 25–32.
[3] J.-H. Yang, Y.-S. Han, M. Park, T. Park, S.-J. Hwang, J.-H. Choy, New inorganic-bsed drug delivery system of indole-3-acetic acid-layered metal hydroxide nanohybrids with controlled release rate, Chem. Mater., 19 (2007) 2679-2685.
[4] M.D. Arco, E. Cebadera, S. Gutiérrez, C. Martín, M. Montero, V. Rives, J. Rocha, M. Sevilla, Mg,Al layered double hydroxides with intercalated indomethacin: synthesis, characterization, and pharmacological study, J. Pharm. Sci., 93 (2004) 1649-1658.
[5] B. Ballarina, A. Mignani, F. Mogaveroa, S. Gabbaninic, M. Morig, Hybrid material based on ZnAl hydrotalcite and silver nanoparticles for deodorant formulation, Appl. Clay. Sci., 114 (2015) 303-308.
[6] R.J. Chimentão, S. Abelló, F. Medina, J. Llorca, J.E. Sueiras, Y. Cesteros, P. Salagre, Defect-induced strategies for the creation of highly active hydrotalcites in base-catalyzed reactions, J. Catal., 252 (2007) 249–257.
[7] D.-H. Park, G. Choi, J.-H. Choy, Bio-layered double hydroxides nanohybrids for theranostics applications, Photofunctional Layered Materials2015, pp. 137-175.
[8] N.T. Whilton, P.J. Vickers, S. Mann, Bioinorganic clays: synthesis and characterization of amino- and polyamino acid intercalated layered double hydroxides, J. Mater. Chem., 7 (1997) 1623–1629.
[9] S. Aisawa, S. Takahashi, W. Ogasawara, Y. Umetsu, E. Narita, Direct intercalation of amino acids into layered double hydroxides by coprecipitation, J. Solid State Chem., 162 (2001) 52-62
[10] B.M. Choudary, B. Kavita, N.S. Chowdari, B. Sreedhar, M.L. Kantam, Layered double hydroxides containing chiral organic guests: Synthesis, characterization and application for symmetric C-C bond-formin reactions, Catal. Lett., 78 (2002) 373-377.
[11] Q. Yuan, M. Wei, Z. Wang, G. Wang, X. Duan, Preparation and characterization of L-aspartic acid-intercalated layered double hydroxide, Clays Clay Miner., 52 (2004) 40–46.
[12] M. Wei, J. Guo, Z. Shi, Q. Yuan, M. Pu, G. Rao, X. Duan, Preparation and characterization of L-cystine and L-cysteine intercalated layered double hydroxides, Journal of Materials Science 42 (2007) 2684-2689.
[13] Å. Fudala, I. Pálinkó, B. Hrivnák, I. Kiricsi, Amino acid-pillared layered double hydroxide and montmorillonite thermal characteristics, J. Therm. Anal. Calorim., 56 (1999) 317-322.
[14] Á. Fudala, I. Pálinkó, I. Kiricsi, Amino acids, precursors for cationic and anionic intercalation synthesis and characterization of amino acid pillared materials, J. Mol. Struct., 482-483 (1999) 33-37.
[15] Á. Fudala, I. Pálinkó, I. Kiricsi, Preparation and characterization of hybrid organic-inorganic composite materials using the amphoteric property of amino acids: amino acid intercalated layered double hydroxide and montmorillonite, Inorg. Chem., 38 (1999) 4653-4658.

[16] S. Aisawa, H. Kudo, T. Hoshi, S. Takahashi, H. Hirahara, Y. Umetsu, E. Narita, Intercalation behavior of amino acids into Zn–Al-layered double hydroxide by calcination–rehydration reaction, J. Solid State Chem., 177 (2004) 3987–3994.
[17] H. Nakayama, N. Wada, M. Tsuhako, Intercalation of amino acids and peptides into Mg–Al layered double hydroxide by reconstruction method, Int. J. Pharm., 269 (2004) 469–478.
[18] B. List, R.A. Lerner, C.F.B. III, Proline-catalyzed direct asymmetric aldol reactions, J. Am. Chem. Soc., 122 (2000) 2395-2396.
[19] A. Córdova, W. Zou, I. Ibrahem, E. Reyes, M. Engqvist, W.-W. Liao, Acyclic amino acid-catalyzed direct asymmetric aldol reactions: alanine, the simplest stereoselective organocatalyst, Chem. Commun., (2005) 3586–3588.
[20] X. Wu, Z. Jiang, H.-M. Shen, Y. Lu, Highly efficient threonine-derived organocatalysts for direct asymmetric aldol reactions in water, Adv. Synth. Catal., 349 (2007) 812 – 816.
[21] S.S.V. Ramasastry, K. Albertshofer, N. Utsumi, F. Tanaka, I. Carlos F. Barbas, Mimicking fructose and rhamnulose aldolases: organocatalytic syn-aldol reactions with unprotected dihydroxyacetone, Angew. Chem. Int. Ed., 46 (2007) 5572–5575.
[22] Z. Jiang, Z. Liang, X. Wu, Y. Lu, Asymmetric aldol reactions catalyzed by tryptophan in water, Chem. Commun., (2006) 2801–2803.
[23] X.-Y. Xu, Y.-Z. Wang, L.-Z. Gong, Design of organocatalysts for asymmetric direct syn-aldol reactions, Org. Lett., 9 (2007) 4247-4249.
[24] T. Kanemitsu, A. Umehara, M. Miyazaki, Kazuhiro Nagata, T. Itoh, L-t-leucine-catalyzed direct asymmetric aldol reaction of cyclic ketones, Eur. J. Org. Chem., (2011) 993–997.
[25] F. Orsini, F. Pelizzoni, M. Forte, R. Destro, P. Gariboldi, 1,3 dipolar cycloadditions of azomethine ylides with aromatic aldehydes. Syntheses of 1-oxopyrrolizidines and 1,3-oxazolidines, Tetrahedron, 44 (1988) 519-541.
[26] F. Cavani, F. Triffrò, A. Vaccari, Hydrotalcite-type anionic clays: preparation, properties and applications., Catal. Today, 11 (1991) 173-301.
[27] M.G. Álvarez, R.J. Chimentão, F. Figueras, F. Medina, Tunable basic and textural properties of hydrotalcite derived materials for transesterification of glycerol, Appl. Clay. Sci., 58 (2012) 16-24.
[28] S. Aisawa, S. Sasaki, S. Takahashi, H. Hirahara, H. Nakayama, E. Narita, Intercalation of amino acids and oligopeptides into Zn–Al layered double hydroxide by coprecipitation reaction, J. Phys. Chem. Solids, 67 (2006) 920–925.
[29] A.R. Garcia, R.B.d. Barros, A. Fidalgo, L.M. Ilharco, Interactions of L-alanine with alumina as studied by vibrational spectroscopy, Langmuir 23 (2007) 10164-10175.
[30] N.B. Colthup, L.H. Daly, S.E. Wiberley, Introduction to infrared and raman spectroscopy, 3rd ed.1990.
[31] A. Béres, I. Pálinkó, J.-C. Bertrand, J.B. Nagy, I. Kiricsi, Dehydration-rehydration behaviour of layered double hydroxides: a study by X-ray diffractometry and MAS NMR spectroscopy J. Mol. Struct., 410-411 (1997) 13-16.
[32] J. Rocha, M.d. Arco, V. Rives, M.A. Ulibarri, Reconstruction of layered double hydroxides from calcined precursors: a powder XRD and ^{27}Al MAS NMR study, J. Mater. Chem., 9 (1999) 2499-2503.
[33] F. Rey, V. Fornéa, Thermal decomposition of hydrotalcites an infrared and nuclear magnetic resonance spectroscopic study, J. Chem. Soc., Faraday Trans., 88 (1992) 2233-2238.
[34] K.T. Barrett, A.J. Metrano, P.R. Rablen, S.J. Miller, Spontaneous transfer of chirality in an atropisomerically enriched two-axis system, Nature, 509 (2014) 71-75.
[35] E. Dumitriu, V. Hulea, C. Chelaru, C. Catrinescu, D. Tichit, R. Durand, Influence of the acid–base properties of solid catalysts derived from hydrotalcite-like compounds on the condensation of formaldehyde and acetaldehyde, Appl. Catal., A, 178 (1999) 145-157.
[36] S. Paladhi, A. Chauhan, K. Dhara, A.K. Tiwari, J. Dash, An uncatalyzed aldol reaction of thiazolidinedione, Green. Chem., 14 (2012) 2990–2995.

[37] Y. Hayashi, In water or in the presence of water?, Angew. Chem. Int. Ed., 45 (2006) 8103 – 8104.
[38] A.P. Brogan, T.J. Dickerson, K.D. Janda, Enamine-based aldol organocatalysis in water: Are they really “all wet”?, Angew. Chem. Int. Ed., 48 (2006) 8100 – 8102.
[39] A. Bassan, W. Zou, E. Reyes, F. Himo, A. Córdova, The origin of stereoselectivity in primary amino acid catalyzed intermolecular aldol reactions, Angew. Chem. Int. Ed., 44 (2005) 7028 – 7032.
[40] M. Amedjkouh, Aqua-organocatalyzed direct asymmetric aldol reaction with acyclic amino acids and organic bases with control of diastereo- and enantioselectivity, Tetrahedron: Asymmetry, 18 (2007) 390–395.
[41] X.-H. Chen, J. Yu, L.-Z. Gong, The role of double hydrogen bonds in asymmetric direct aldol reactions catalyzed by amino amide derivatives, Chem. Commun., 46 (2010) 6437–6448.
[42] M. Kakihana, T. Nagumo, M. Okamoto, H. Kakihana, Coordlnatlon structures for uranyl carboxylate complexes in aqueous solution studied by IR and ^{13}C NMR Spectra J. Phys. Chem. B, 91 (1987) 6128-6136.
[43] P. Zhou, S. Luo, J.-P. Cheng, Highly enantioselective synthesis of syn-aldols of cyclohexanones via chiral primary amine catalyzed asymmetric transfer aldol reactions in ionic liquid, Org. Biomol. Chem., 9 (2011) 1784–1790.
[44] B. Rodríguez, A. Bruchmann, C. Bolm, A highly eficient asymmetric organocatalytic aldol reaction in a ball Chem. Eur. J., 13 (2007) 4710 – 4722.
[45] L. Li, S. Gou, F. Liu, Highly stereoselective anti-aldol reactions catalyzed by simple chiral diamines and their unique application in configuration switch of aldol products, Tetrahedron Lett., 54 (2013) 6358–6362.

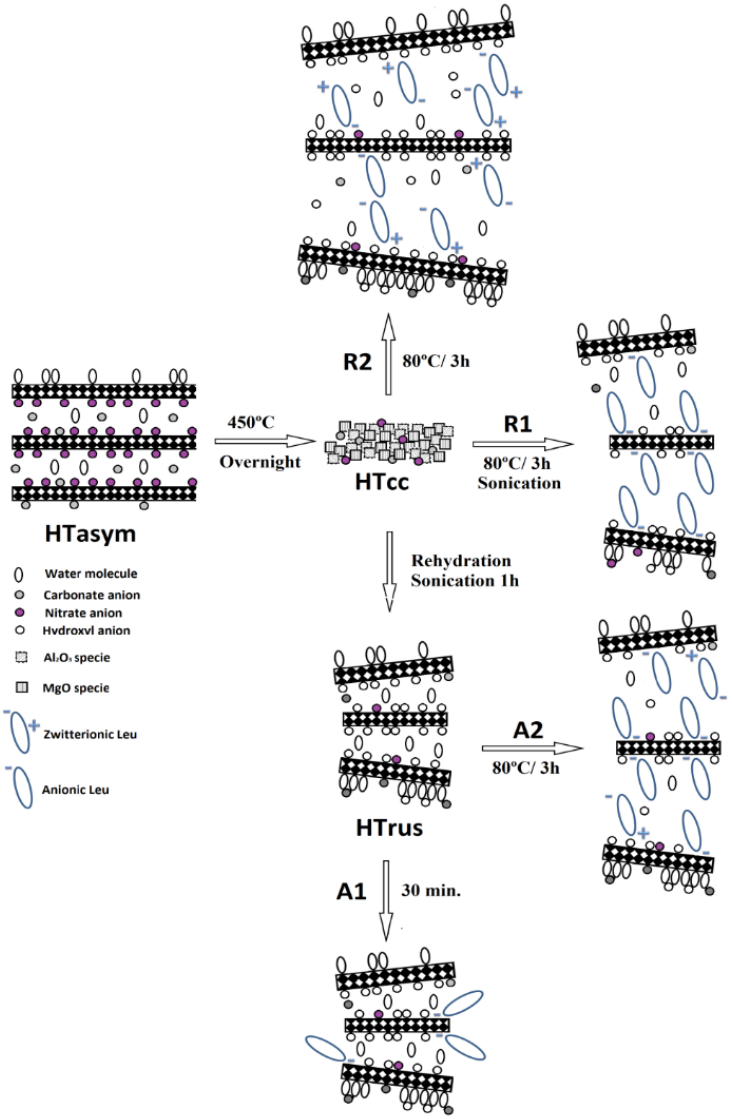

Scheme 1. Schematic representation of the LL/HT materials obtained by the different protocols. L-Leu is immobilized in both zwitterion and anionic form in method A2 and only in anionic form in method R1.

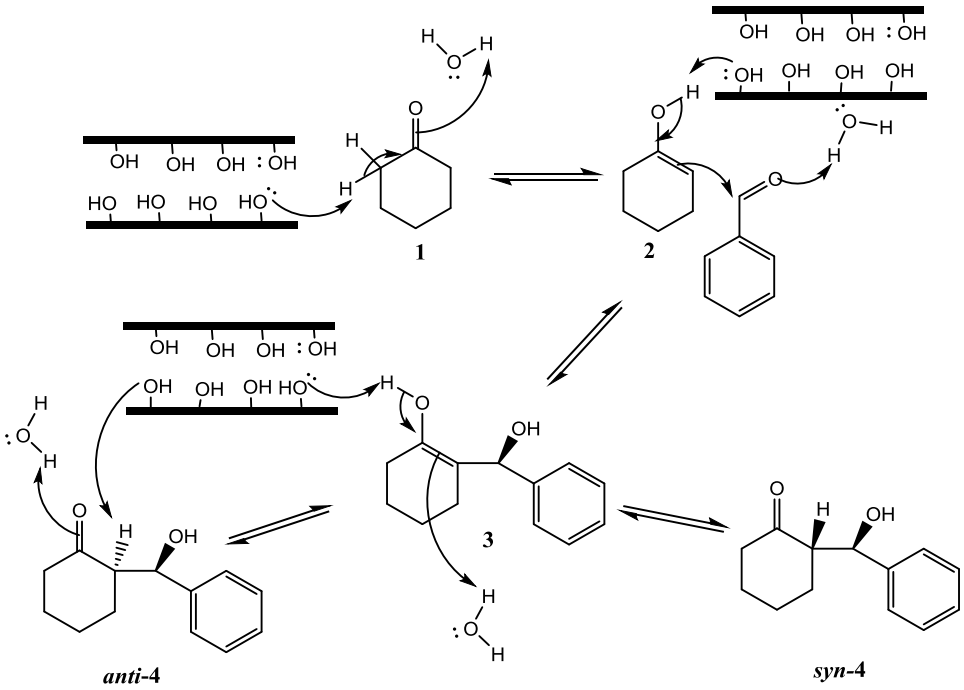

Scheme 2. Possible mechanism for the *syn-anti* isomerization

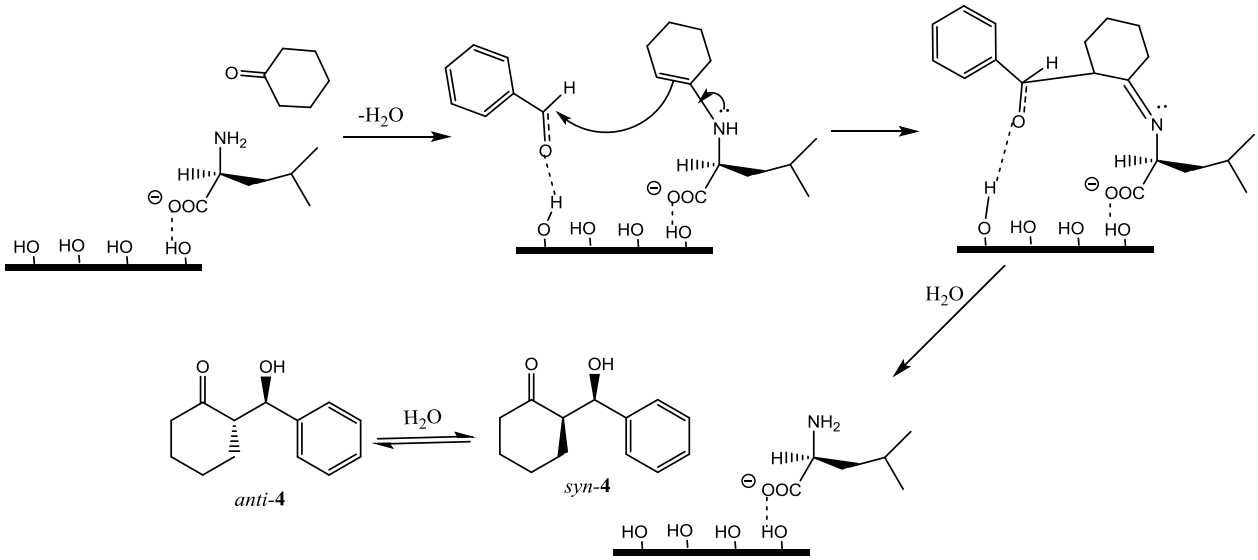

Scheme 3. Proposed enamine-type mechanism for the aldol reaction catalysed by LL/HT_{rus} (both R1 and A2) catalysts.

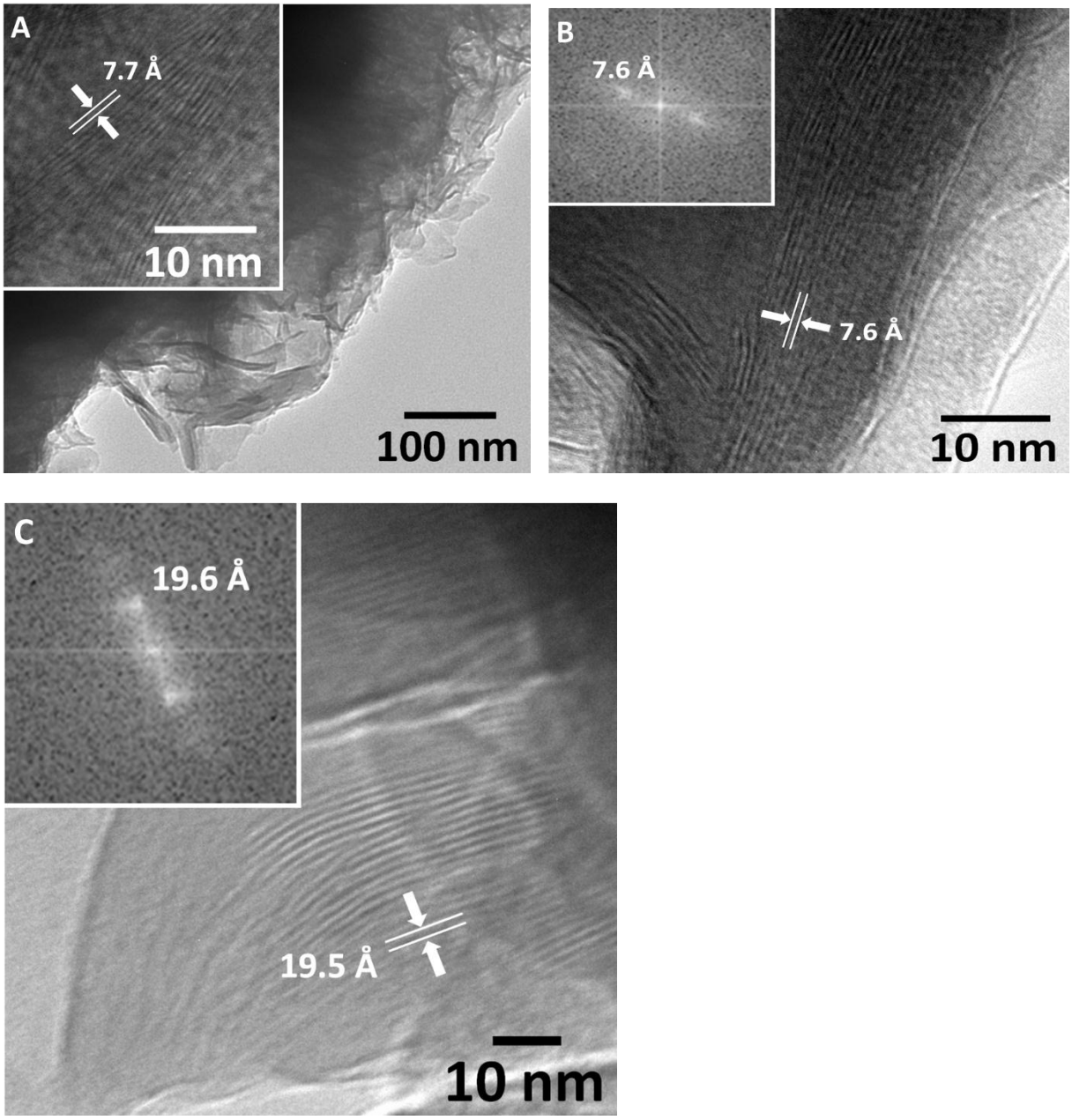

Figure 1. HRTEM images of the nanohybrids synthesized by anionic-exchange method: a) HT_{rus}, b) LL/HT_{rus}-A1 and c) LL/HT_{rus}-A2.

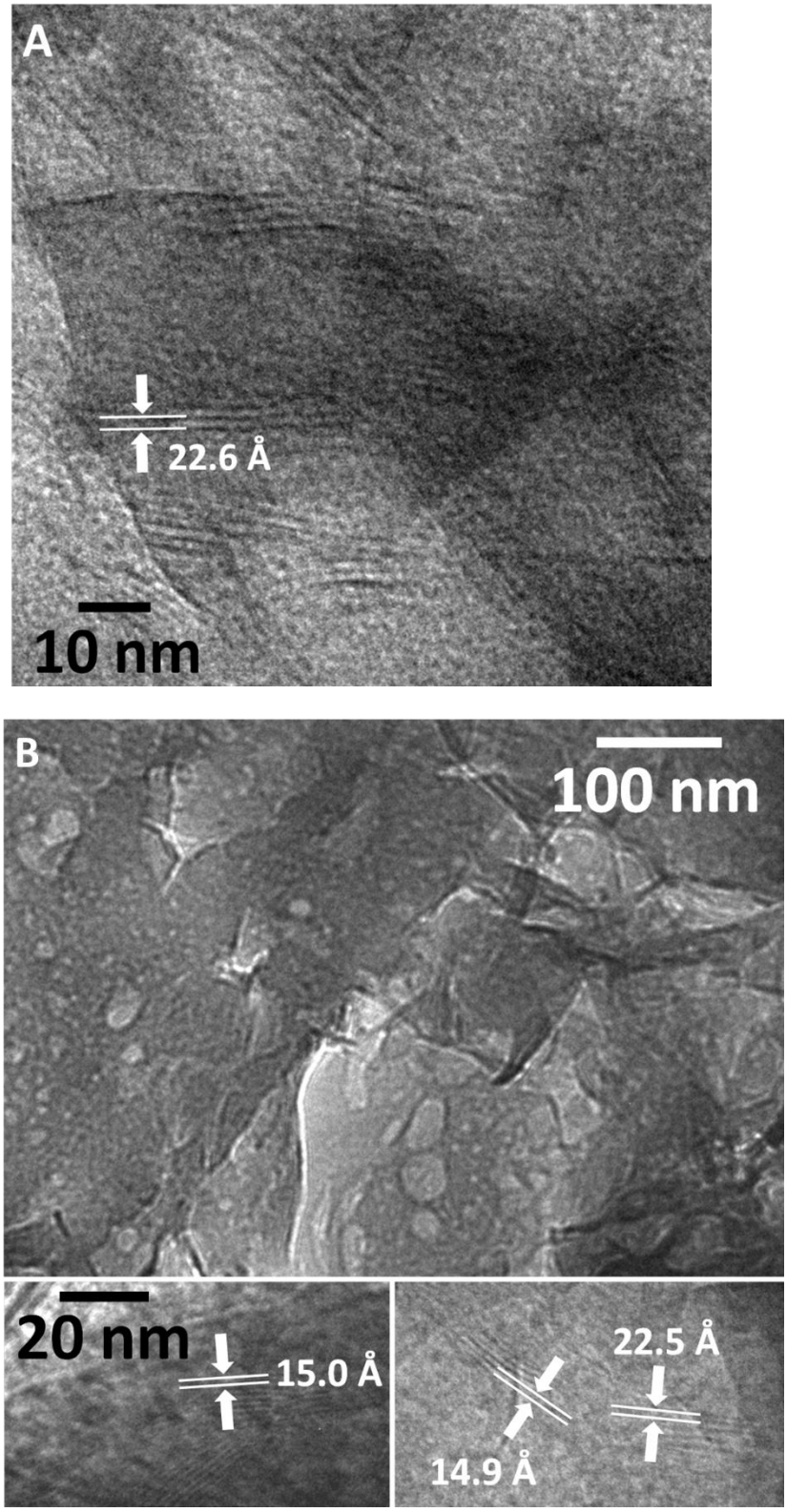

Figure 2 HRTEM images of the nanohybrids synthesized by the reconstruction method: a) LL/HT_{rus}-R1 and b) LL/HT_r-R2.

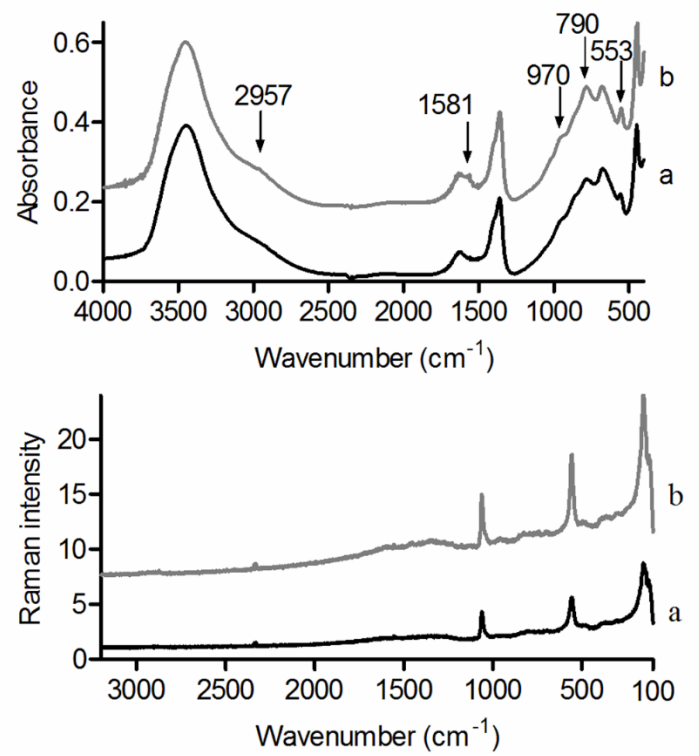

Figure 3. Skeletal FT-IR (up) and Raman (bottom) spectra of a) LL/HT_{Clus}-A1, b) LL/HT_{Clus}-A2.

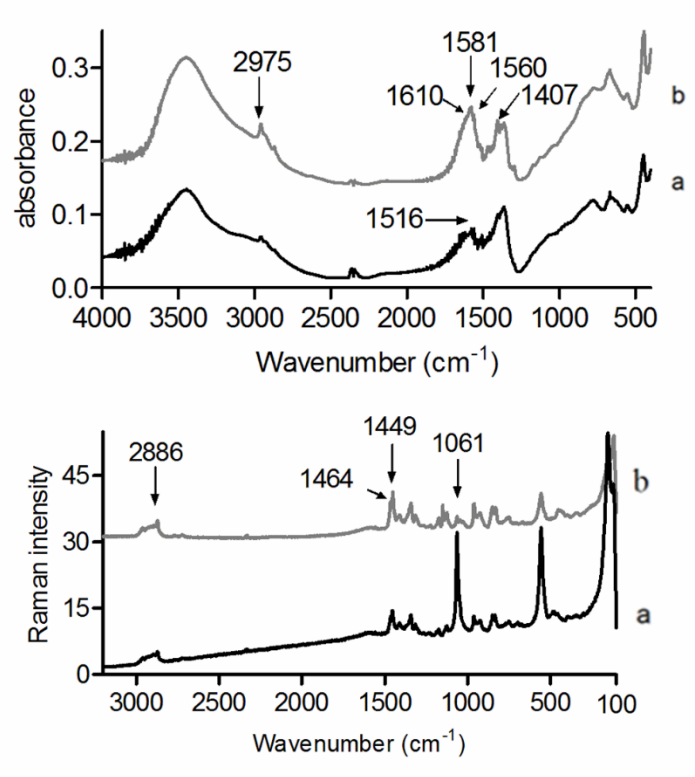

Figure 4. Skeletal FT-IR (up) and Raman (bottom) spectra of a) LL/HT_{rus}-A1 and b) LL/HT_{rus}-A2.

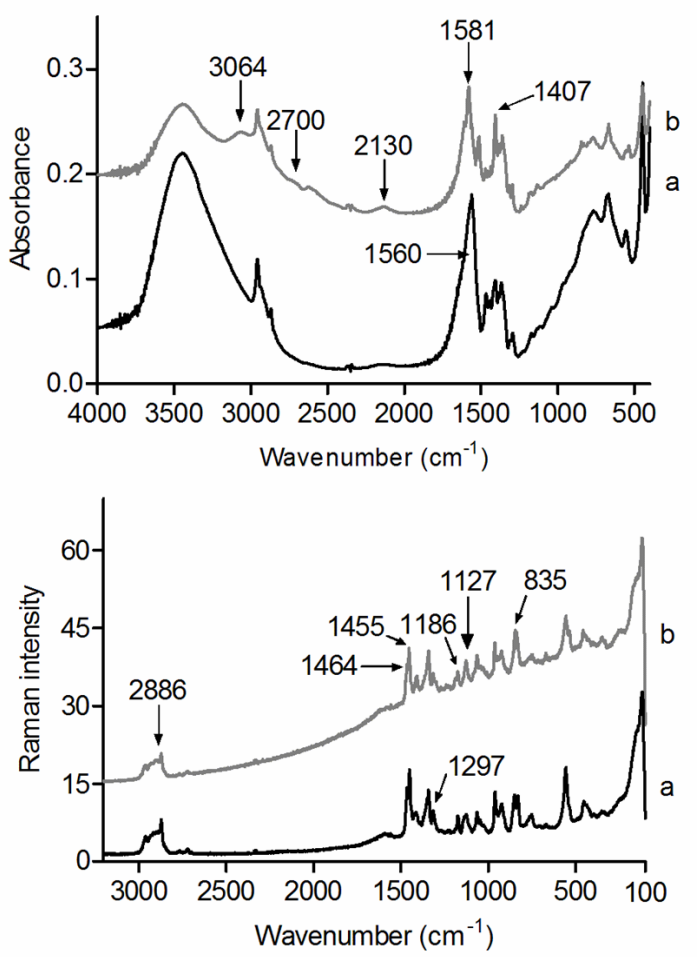

Figure 5. Skeletal FT-IR (up) and Raman (bottom) spectra of a) LL/HT_{rus}-R1 and b) LL/HT_{r}-R2.

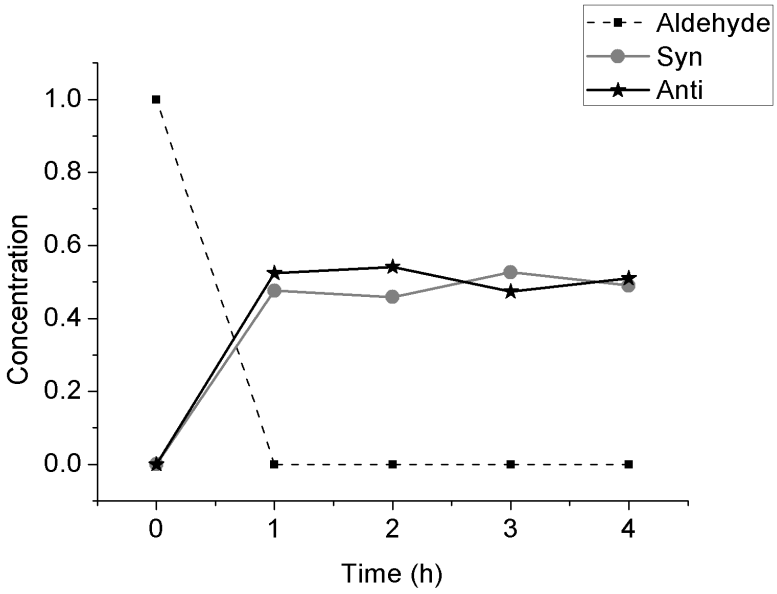

Figure 6. First 4h of reaction: Reaction conditions: benzaldehyde (0.5 mmol), cyclohexanone (1.5 mmol), catalyst HT rehydrated in DMSO (2 ml) and H_2O (25 mmol); result obtained from ^{1}H-NMR spectra.

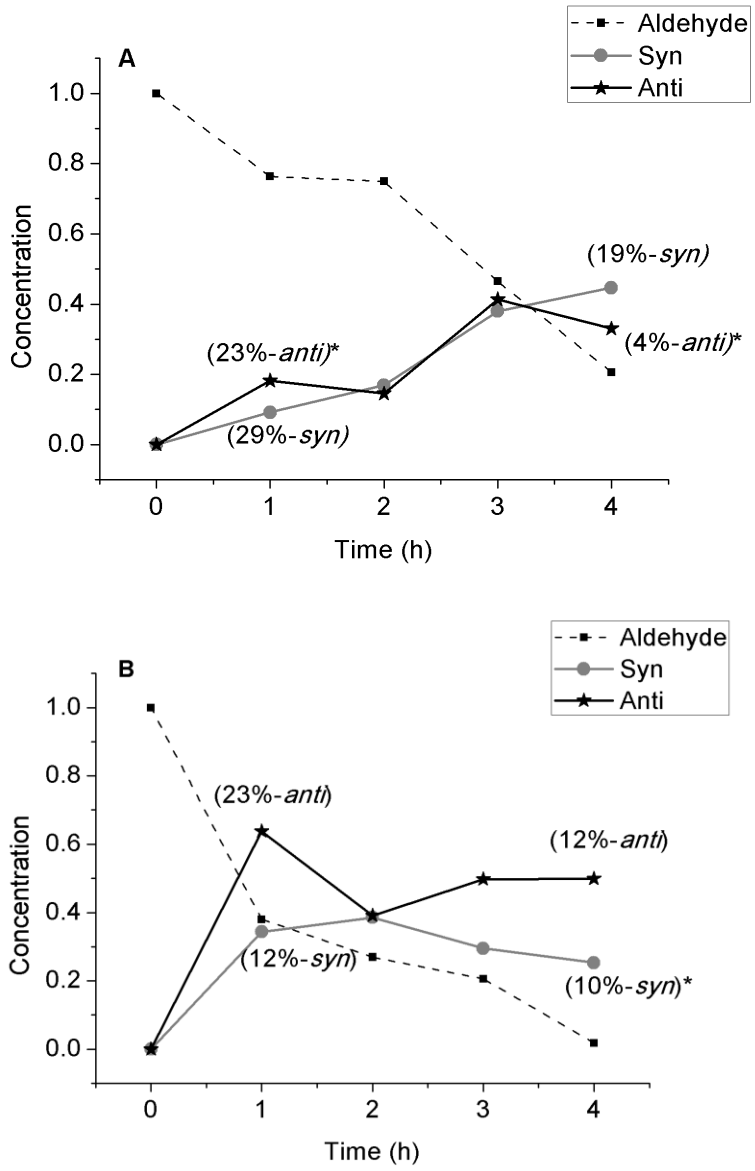

Figure 7. First 4h of reaction: A) – HT_c+ L-Leu ; B) - HT_{rus} + L-Leu. Reaction conditions: benzaldehyde (0.5 mmol), cyclohexanone (1.5 mmol), catalyst (2.5 mol % L-Leucine with respect to ketone) in DMSO (2 ml) and H_2O (25 mmol); result obtained from ^{1}H-NMR spectra. *The other enantiomer was obtained.

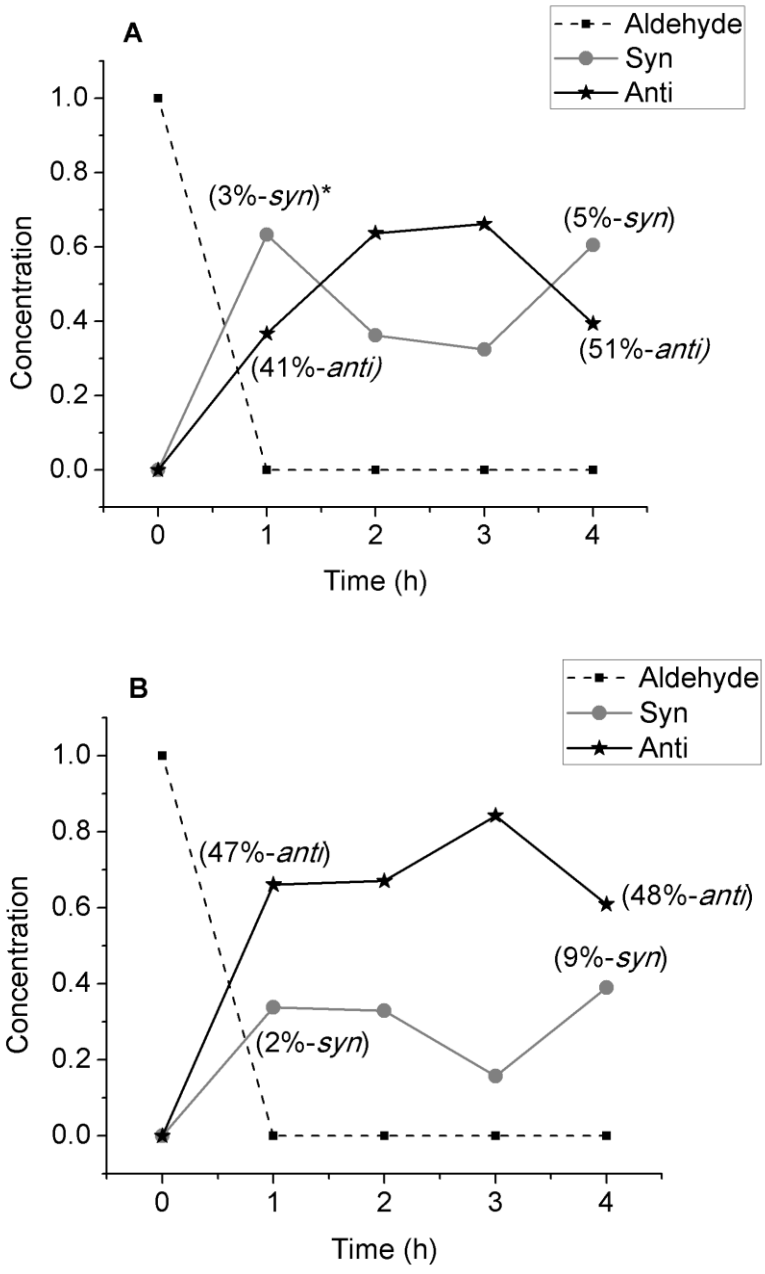

Figure 8. First 4h of reaction: A) – LL/HT_{rus}-A2, B) - LL/HT_{rus}-R1. Reaction conditions: benzaldehyde (0.5 mmol), cyclohexanone (1.5 mmol), catalyst (2.5 mol % L-Leucine with respect to ketone) in DMSO (2 ml) and H_2O (25 mmol); result obtained from ^{1}H-NMR spectra. *The other enantiomer was obtained.

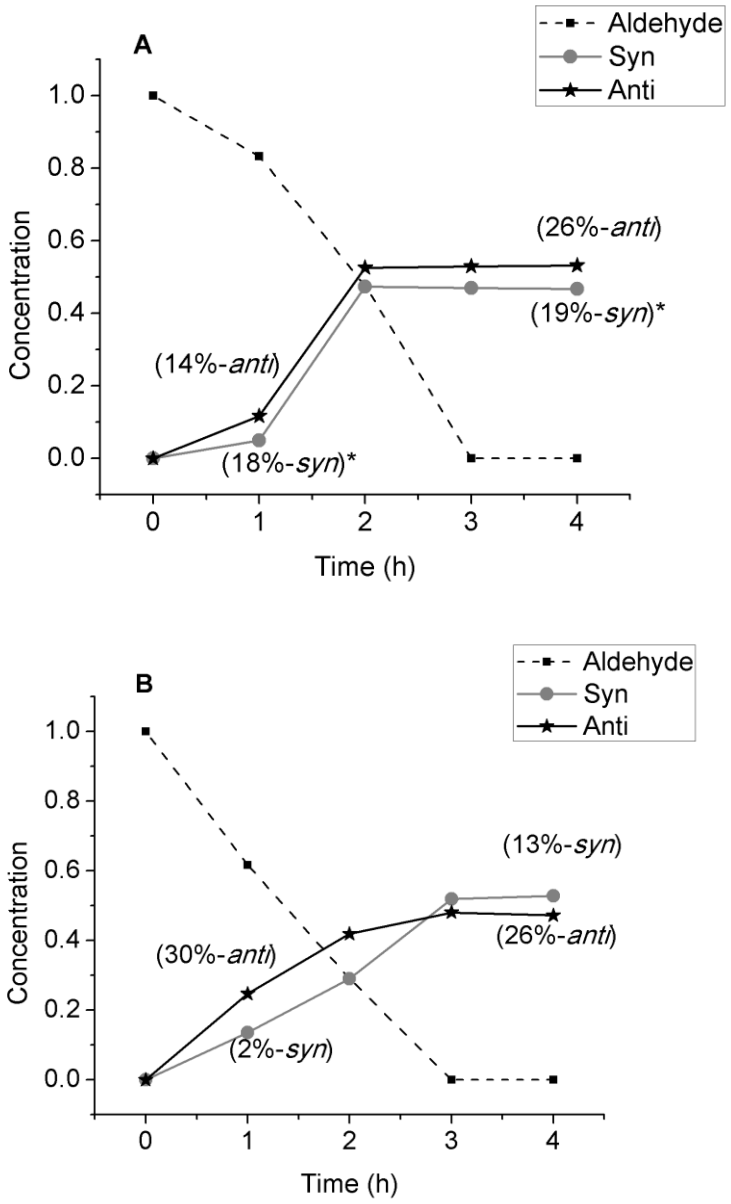

Figure 9. First 4h of reaction: A) – LL/HT_{rus}-A2 B) - LL/HT_{rus}-R1. Reaction conditions: benzaldehyde (0.5 mmol), cyclohexanone (1.5 mmol), catalyst (2.5 mol % L-Leucine with respect to ketone) in toluene (2 ml); result obtained from ^{1}H-NMR spectra. *The other enantiomer was obtained.

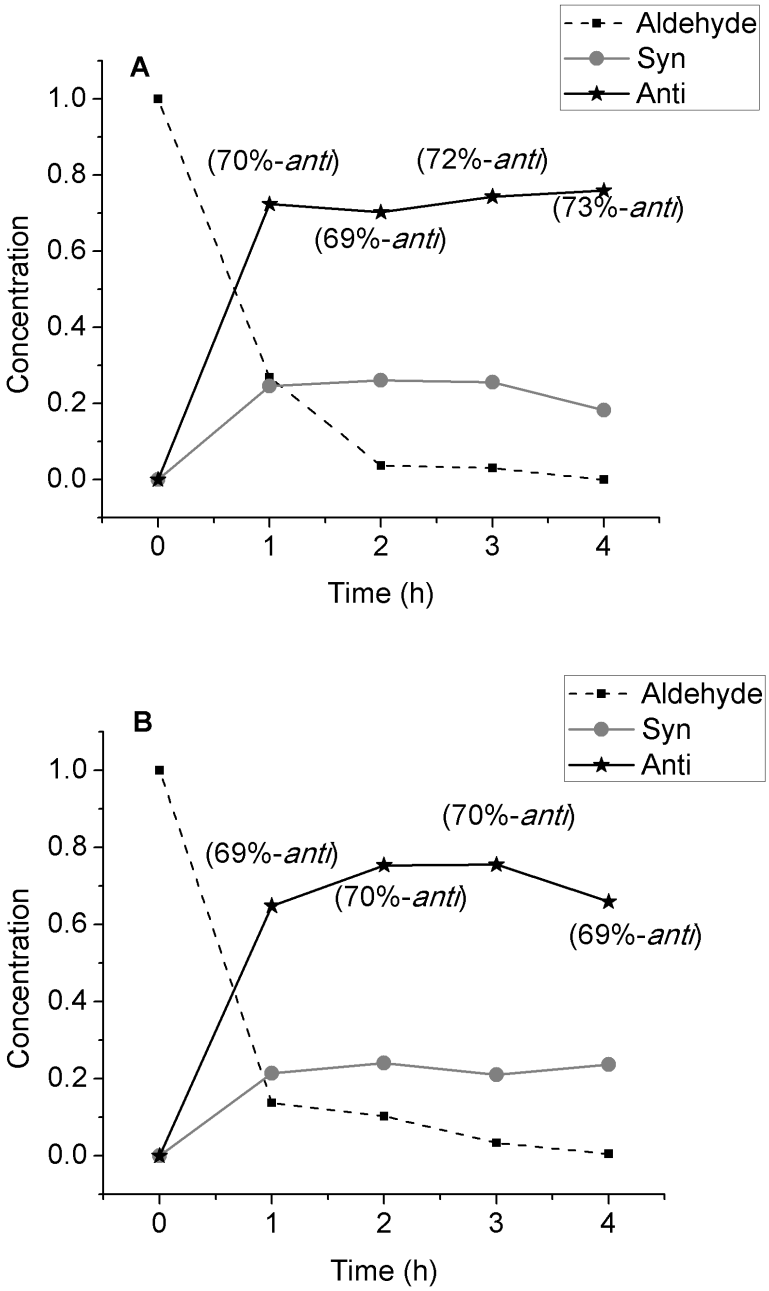

Figure 10. First 4h of reaction: A) – LL/HT_{rus}-A2 B) - LL/HT_{rus}-R1. Reaction conditions: benzaldehyde (0.5 mmol), cyclohexanone (1.5 mmol), catalyst (2.5 mol % L-Leucine with respect to ketone) in toluene (2 ml) and H_2O (25 mmol); result obtained from ^{1}H-NMR spectra.

Tables

Table 1 Summary of the synthesis methods

Method	**Variations**	**Material**
Anionic exchange (A) *500 mg HT* *L-Leu* *HT = HT_{rus} or HT_{Cl}*	A1 *30 min, r.t.* *2.4mmol L-Leu*	LL/HT_{rus}-A1 LL/HT_{Clus}-A1
	A2 *3h; 80ºC* *6.4 mmol L-Leu*	LL/HT_{rus}-A2 LL/HT_{Clus}-A2
Reconstruction (R) *250 mg HT_{cc}* *6.4 mmol L-Leu* *80ºC, 3h*	R1 *(previous sonication 1h)*	LL/HT_{rus}-R1
	R2	LL/HT_{r}-R2

Table 2. Characterization data of HT and LL/HT materials

Entry	Material	L-Leu/Al molar ratio[a)]	Interlayer space d_{003} (Å)[b)]	Gallery height (Å)[c)]	BET surface area (m^2/g)
1	HT_{NO3}	-	8,4	3,6	56
2	HT_{cc}	-	-	-	188
3	HT_{rus}	-	7.7	2.9	40
4	HT_{Clus}	-	7,9	3,1	55
5	LL/HT_{rus}-A1	0.44	7,7	2,9	12
6	LL/HT_{Clus}-A1	0.04	7,9	3,1	43
7	LL/HT_{rus}-A2	1.09	19,5	14,3	14
8	LL/HT_{Clus}-A2	0.16	7,9	3,1	30
9	LL/HT_{rus}-R1	0.95	20,0	15,2	10
10	LL/HT_{r}-R2	0.92	21,2	16,4	8

[a)]Calculated by EA and ICP analysis. [b)]In all cases, the materials obtained exhibit the characteristic diffraction peaks of the meixnerite structure (JCPDS 35-0965).[c)]Gallery height was calculated on the basis of Aisawa *et al.* calculations [9] where the Mg/Al layer has a total height of 4.8 Å.

Table 3. Summary of characterization data for the LL/HT materials

Material	Method	L-Leu location in the HT[a)]	$\nu_{a(COO-)}$ [b)]	$\nu_{s(COO-)}$ [b)]	$\Delta\nu$ [c)]	L-Leu structure[d)]	Kind of interaction[e)]
L-Leu	-	-	1581	1407	174	Z	-
LL/HT_{Clus}-A1 [f)]	A1	-	-	-	-	-	-
LL/HT_{Clus}-A2 [f)]	A2	-	-	-	-	-	-
LL/HT_{rus}-A1	A1	Edges	1560	1408	152	A	Bridging
LL/HT_{rus}-A2	A2	Interlayer space	1560	1408	152	A	Bridging
			1581	1408	173	Z	H-bonding
LL/HT_{rus}-R1	R1	Interlayer space	1560	1407	153	A	Bridging
LL/HT_{r}-R2	R2	Interlayer space	1581	1407	174	Z	H-bonding

[a)]Determined by XRD analysis. [b)]Determined directly from the FT-IR spectra. [c]$\Delta\nu = \nu_{a(COO-)} - \nu_{s(COO-)}$. [d)]Based on the presence of NH_3^+ group by FT-IR. Z= zwitterionic and A= Anionic. [e)]Host-guest interaction based on the FTIR spectra: $\Delta\nu L_{-Leu} > \Delta\nu_{nanohyb.}$ = bidentate interaction; $\Delta\nu_{L-Leu} < \Delta\nu_{nanohyb.}$ = bridging interaction. According to Nakamoto.[42] [f)]Undetected immobilized L-Leu

Table 4. ^{27}Al-MAS and ^{13}C MAS NMR characterization of LL/HT nanohybrid materials

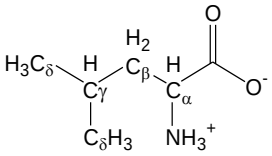

Entry	Material	Al_{oh}	COO^-	C_α	C_β	C_γ	C_δ
1	L-Leu	-	176	55	44	26	26
2	LL/HT_{rus}-A2	9	186 177[a)]	56	48	27	24
3	LL/HT_{rus}-R1	9	186	58	49	27	25
4	LL/HT_r-R2	9	177 186[a)]	56	48	27	25

[a)]Less intense signal

Table 5. Asymmetric Aldol Reaction of Cyclohexanone

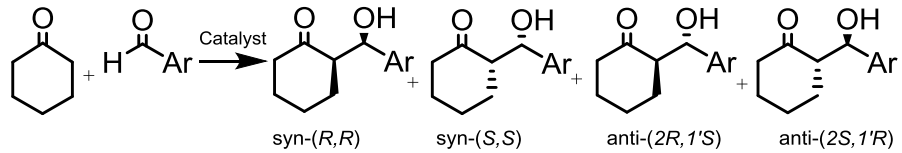

Entry[a)]	Ar	Catalyst	Yield [%][b)]	*dr*[b)] (*syn/anti*)	*ee* of syn[c)] [%]	*ee* of anti[c)] [%]
1[d)]	4-$NO_2C_6H_4$	L-Leu	16	1:3.4	N.D.	82 [d)]
2		HT_{rus}	99	64:36	-	-
3		LL/HT_{rus}-R1	99	58:42	90	60
4		LL/HT_{rus}-A2	94	61:39	71	74
5	2-$NO_2C_6H_4$	HT_{rus}	96	63:37	-	-
6		LL/HT_{rus}-R1	80	53:47	60	98
7		LL/HT_{rus}-A2	91	56:44	36	91
8	4-ClC_6H_4	HT_{rus}	97	53:47	-	-
9		LL/HT_{rus}-R1	80	56:44	49	86
10		LL/HT_{rus}-A2	80	59:41	38	87
11	C_6H_5	HT_{rus}	99	44:56	-	-
12		LL/HT_{rus}-R1	99	54:46	50	74
13		LL/HT_{rus}-A2	94	43:57	5 *	0
14		HT_{cc} + LL	85	46:54	10	28
15		HT_{rus} + LL	99	48:52	27*	38

[a)]Standard conditions: corresponding benzaldehyde (0.5 mmol), cyclohexanone (1.5 mmol), catalyst (2.5 mol % L-Leucine with respect to ketone) in DMSO (2 ml) and H_2O (25 mmol) for 7 days. Brine was added over the reaction mixture and the organic layer was extracted with dichloromethane. [b)]Determined by either isolation or ^1H NMR based on ref [24, 43].[c)]Determined by HPLC based on ref.[43-45].[d)]From ref. [24] *The other *syn*-enantiomer was obtained.

Table 6. Stability and Reusability of the Heterogeneous Catalyst in Asymmetric Aldol Reaction of Benzaldehyde with Cyclohexanone

Entry	Solvent	Catalyst	Run	Yield [%][c)]	*dr*[c)] (*syn/anti*)	*ee* of syn[d)] [%]	*ee* of anti[d)] [%]
1	DMSO[a)]	L-Leu/HT_{rus}-A2	1	94	43:57	5*	0.4
			2	-	-	-	-
			3	-	-	-	-
2	DMSO[a)]	L-Leu/HT_{rus}-R1	1	93	47:53	50	74
			2	99	32:68	83	13
			3	-	-	-	-
3	Toluene[b)]	L-Leu/HT_{rus}-A2	1	99	43:57	10*	22
			2	97	41:59	18*	32
			3	99	40:60	33*	46
4	Toluene[b)]	L-Leu/HT_{rus}-R1	1	76	37:63	15*	18
			2	84	40:60	7*	22
			3	99	45:55	8*	17

[a)]Reaction conditions: benzaldehyde (0.5 mmol), cyclohexanone (1.5 mmol), catalyst (2.5 mol % L-Leucine with respect to ketone) in DMSO (2 ml) and H_2O (25 mmol) for 7 days. Brine was added over the reaction mixture and the organic layer was extracted with dichloromethane. [b)]Reaction conditions: benzaldehyde (0.5 mmol), cyclohexanone (1.5 mmol), catalyst (2.5 mol % L-Leucine with respect to ketone) in Toluene (2 ml) ;[c)]Determined by either isolation or ^{1}H-NMR based on ref [24, 43].[d)]Determined by HPLC based on ref. [43-45] *The other *syn*-enantiomer was obtained.